

Pressure and shear waves in lightly-confined granular columns

Vasu Paliwal^{1,*}, Kokkonda Vikas^{1,**}, Hiroaki Katsuragi^{3,***}, Deepak Dhingra^{4,****}, and Ishan Sharma^{1,2,†}

¹Department of Mechanical Engineering, IIT Kanpur, Kanpur, India

²Department of Space, Planetary & Astronomical Sciences and Engineering, IIT Kanpur, Kanpur, India

³Department of Earth and Space Science, Osaka University, Osaka, Japan

⁴Department of Earth Science, IIT Kanpur, Kanpur, India

Abstract. Waves in lightly confined granular media find application in extraterrestrial scenarios involving small bodies like asteroids where the gravitational pressures can be as low as a few pascals, as in the case of Itokawa. We report findings from discrete element (DE) simulations of pressure (P) and shear (S) wave transmissions through very lightly confined granular columns. We consider both monodisperse and bidisperse granular aggregates. Waves are excited in various ways, e.g., by a continuously driven wall at one end of the column, a short pulse, or a sinusoidal input. Our DE simulations are conducted on LAMMPS and were validated against the recent simulations on P waves [Sánchez, P, DJ Scheeres and AC Quillen 2022. Transmission of a seismic wave generated by impacts on granular asteroids. Planet. Sci. J. 3: 245].

1 Introduction

Several space missions to different asteroids of the solar system over the decades have shown that these bodies are composed of regolith particles bound under low confining pressures in microgravity environments ($\approx 10^{-5} \text{ m/s}^2$). The study of wave propagation in extremely low confining environments is crucial for a better understanding of sub-surface and surface phenomena such as size-based segregation of particles on asteroid surfaces.

It has been shown that seismic wave velocity in low confinement pressure depends greatly on the pressure induced by the wave itself [1]. Here, we continue those studies for S and P pulses and try to investigate the potential transition of an S wave into a P wave in lightly confined granular columns.

2 Numerical Simulations and Setup

For our numerical SSDEM (soft-sphere discrete element method) simulations, we utilized LAMMPS [2], an open-source molecular dynamics simulator. The particles are modeled as perfect spheres of varying radii (0.01m - 0.015m in uniform distribution).

The material properties of the particles are chosen to approximate those of LL chondrites, with Young's modulus $E = 2.1 \times 10^{10} \text{ Pa}$ and a Poisson's ratio $\nu = 0.25$. The density of the particles is 3200 kg/m^3 . A simulation

timestep of $1 \times 10^{-6} \text{ s}$ is employed. This choice was validated against the characteristic Hertzian collision time t_c , which was calculated using the expression [3, 4]:

$$t_c = 2.214 \left(\frac{\rho}{E_{\text{eff}}} \right)^{2/5} \frac{d}{v_0^{1/5}} \quad (1)$$

Using E , ν , ρ , particle diameter $d=0.002 \text{ m}$, and impact speed $v_0 = 1500.0 \text{ m/s}$ (maximum velocity of the oscillating piston), we find $t_c \approx 2 \times 10^{-5} \text{ s}$. Our timestep is an order of magnitude lower than t_c , providing sufficient temporal resolution for collision dynamics.

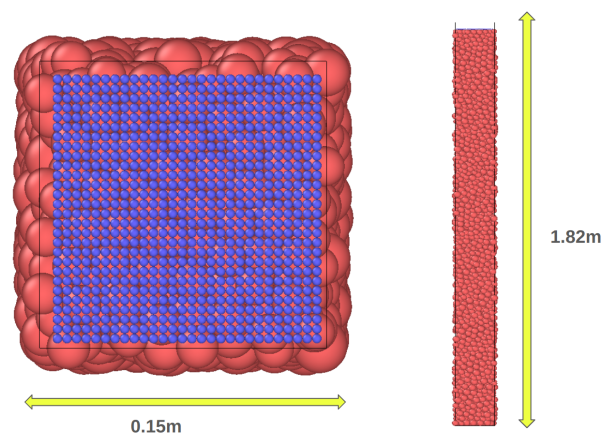


Figure 1. Top and side views of the granular column after bed preparation, showing the piston (in blue) composed of discrete particles. The side and top views are presented at different scales for clarity. The granular column is confined within a container with a square base of $0.15\text{m} \times 0.15\text{m}$ and a height of 1.82m .

*e-mail: vasup20@iitk.ac.in

**e-mail: vikaskok@iitk.ac.in

***e-mail: katsuragi@ess.sci.osaka-u.ac.jp

****e-mail: ddhingra@iitk.ac.in

†e-mail: ishans@iitk.ac.in

2.1 Column Preparation

Particles are confined in a column with a solid base (0.15×0.15 m) and periodic lateral boundaries. Initially, the particles are arranged in a rectangular lattice with a spacing 1.01 times the maximum particle diameter. The particles are then given random initial velocities up to 1 m/s and allowed to settle under gravity with viscous damping to allow the particles to settle quickly by removing the excess kinetic energy.

In the simulations, the piston is constructed from smaller discrete particles with radii one-fourth the size of the smallest particles in the granular bed. This design increases the surface roughness at the contact interface, preventing slip and ensuring that the motion of the piston is effectively transmitted to the adjacent grains. The use of smaller particles also increases the number of contact points, distributing the applied load more uniformly across the granular column and promoting consistent transmission of both normal and tangential forces.

After this, the gravitational force on the particles is removed, and a rough piston composed of smaller particles (with a radius 1/4 of the smallest particles in the bed) is used to compress the granular column to the desired confinement pressure. To achieve this, the piston is constrained to move along the column, and the magnitude of force along the longitudinal direction is determined based on the desired confinement pressure. The system is allowed to evolve, and over time, the bed settles, and the desired confinement pressure is achieved. A packing fraction of 0.65 was achieved after completing this process, close to RCP.

Subsequently, we validated our simulations with those of Sanchez et.al[1]. Comparisons were made for constant velocity compression of granular column at various confinement pressures ranging from 0.1 Pa to 50 kPa. Figure 2 shows the results of our comparative study, which demonstrate good agreement with previously reported trends.

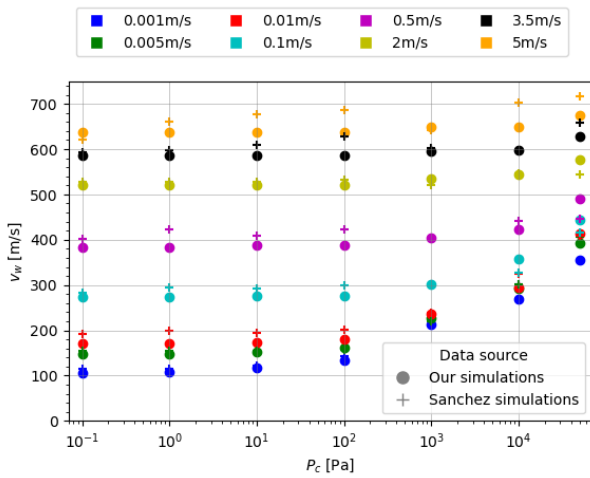


Figure 2. Comparative plot of wave velocity (v_w) versus confinement pressure (P_c) from DEM simulations. Colors indicate piston compression speed; circles represent results from the present study, and plus markers ('+') correspond to Sánchez et al. (2022)

2.2 Wave Initiation

After the preparation of the column at the desired confinement pressure, P and S pulses are imparted to the column. For P pulses, we move the piston in the longitudinal direction, whereas for the S impulse, the first few layers of grains are made to move in the lateral direction. In general, we impart a single pulse of time period $42 \mu\text{sec} \approx 24$ kHz for both S and P waves. For P waves, the motion of the piston as follows:

$$y(t) = y(0) + A \sin(2\pi ft) \quad (2)$$

Whereas for S-waves, the first few layers of particles are moved in the transverse (x) direction as:

$$x(t) = x(0) + A \sin(2\pi ft) \quad (3)$$

In this study, pulse amplitudes of 0.01, 0.05, 0.1, 0.5, 1, 2, 5, and 10 mm are employed, with confining pressures ranging from 100 Pa to 50,000 Pa.

3 Post-Processing and Wave Velocity Measurements

The data for all particles in the column are recorded in dump files at intervals of $4 \mu\text{s}$, corresponding to every four simulation time steps. This high temporal resolution enables detailed probing of the micro-mechanical behavior during wave propagation. This lasts 4 ms, providing enough time for the waves to reach the bottom wall.

We have divided the granular column into 25 bins or slices along its length to analyze the moving wavefront. These slices are roughly 3-4 particle diameters thick. The particles at the interface of two bins are assigned a bin in which their center lies.

3.1 Energy Computations

We performed several computations of the particles over the bin. We computed the translational kinetic energy, rotational kinetic energy, and potential energy stored in particles as they behave like Hertzian springs. We also separately store the inter-particle potential energy (interactions across and the wall particle potential energy (due to particles getting compressed against the bottom wall)). In the present study, however, we consider only the potential energy stored in the normal (compressive) contact springs, excluding contributions from tangential interactions.

The potential energy arises from the elastic Hertzian contacts between particle pairs, modeled using the non-linear Hertzian contact law. The normal contact force between two interacting particles is given by:

$$\mathbf{F}_{ne,Hertz/material} = \frac{4}{3} E_{\text{eff}} R_{\text{eff}}^{1/2} \delta_{ij}^{3/2} \mathbf{n} \quad (4)$$

where E_{eff} is the effective Young's modulus, R_{eff} is the effective radius, δ_{ij} is the normal overlap between particles i and j , and \mathbf{n} is the unit normal vector at the point of contact.

The effective radius is computed as:

$$R_{\text{eff}} = \frac{R_i R_j}{R_i + R_j} \quad (5)$$

For particle–wall interactions (such as with the bottom wall), it simplifies to:

$$R_{\text{eff}} = R_i \quad (6)$$

Thus, the pairwise potential energy stored in the normal Hertzian contact spring between particles i and j is given by:

$$U_{ij} = \frac{2}{5} \times \frac{4}{3} E_{\text{eff}} R_{\text{eff}}^{1/2} \delta_{ij}^{5/2} \quad (7)$$

For each bin, the kinetic energy is computed as follows:

$$RKE = \sum_{i=1}^N \frac{1}{2} I_{\text{sphere}_{\text{CM}}} \omega^2 \quad (8)$$

$$TKE = \sum_{i=1}^N \frac{1}{2} m v_{\text{CM}}^2 \quad (9)$$

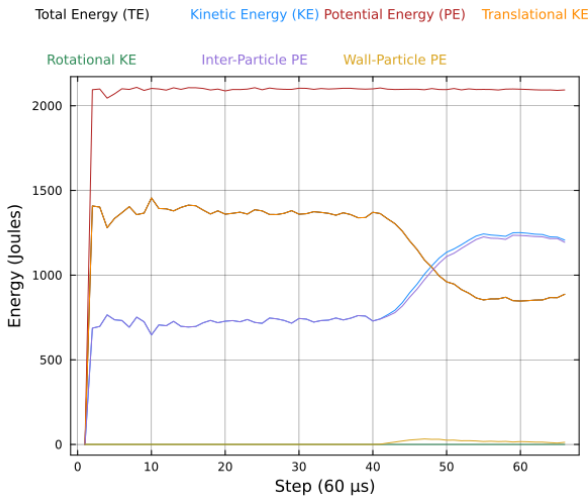


Figure 3. Energy distribution over time in the system, highlighting the rise in potential energy (PE) and decrease in kinetic energy (KE) as the wavefront reaches the wall. Energy components include total energy (TE), KE, PE, translational KE (TKE), rotational KE, inter-particle potential energy (IPPE), and wall-particle potential energy (WPPE). The simulation was conducted for a P wave at a pressure of 1000 Pa and amplitude of 1 mm

3.2 Wave Velocity Measurement

To measure the wave velocities, we track the activity in bins 16 and 7 (out of the 25 equally spaced bins). This choice was arbitrary, and we also conducted trial studies between other bin bounds, obtaining no significant differences in the measured velocity. We use the peak-to-peak approach and mark the arrival times in bins as instances of maximum total kinetic energy for particles in those bins. Since the bin size is known, wave velocity can thus be computed. We then sweep through the entire parameter space.

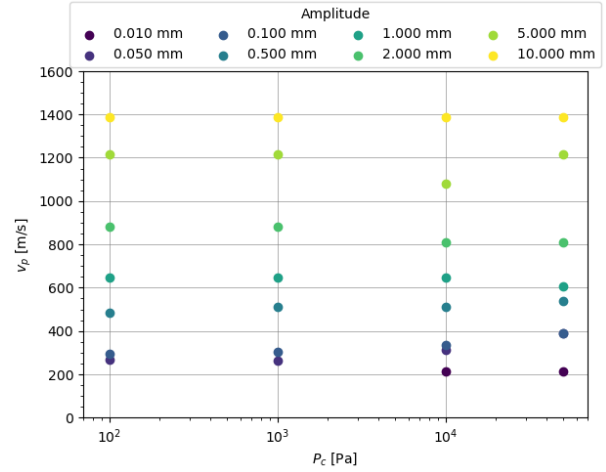


Figure 4. Relationship between P-wave velocity and confining pressure for varying pulse amplitudes.

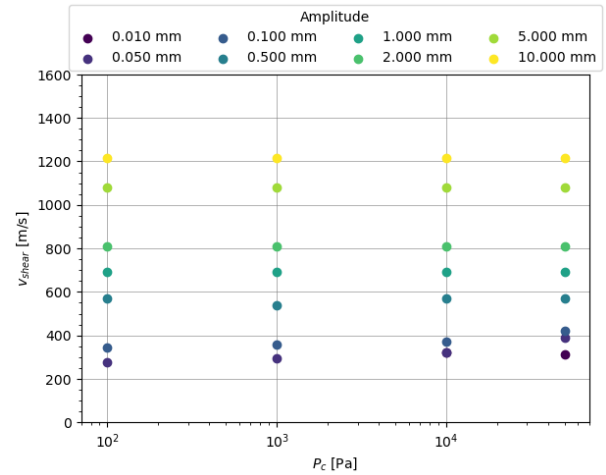


Figure 5. Relationship between S-wave velocity and confining pressure for varying pulse amplitudes

4 Results and Discussions

4.1 Velocities of P and S pulses for different amplitudes

As observed in [1], the velocities of both P and S Pulses are nearly independent of the confining pressure (P_c). They only depend on the pulse amplitude, which influences the induced pressure in the bed. This is clearly demonstrated by points of the same amplitude lying in a straight line for various confining pressures.

Another significant observation is that the velocities of the P and S pulses are nearly identical for the same piston amplitudes. This unexpected result prompted further investigation into the underlying mechanisms.

4.2 Transition of a S wave into a P wave

As we observed identical S and P velocities, we investigated the evolution of the mean velocity profile of the particle. For this, we computed the maximum velocity in each

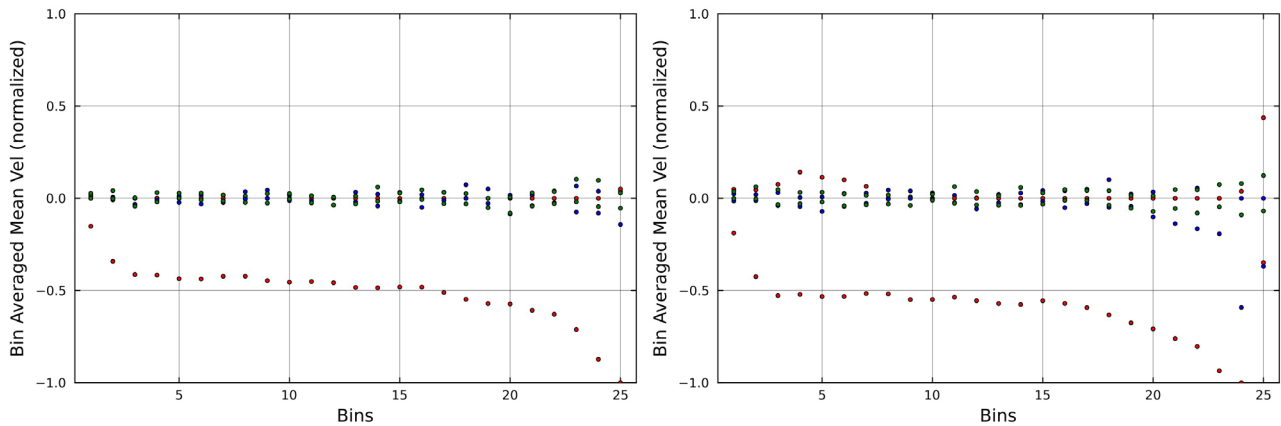


Figure 6. Side-by-side comparison of normalized binwise velocity envelopes of the P pulse (left) and S pulse (right) for $P_c = 1000$ Pa and an amplitude of 0.5 mm. Observe the evolution of v_x (blue), v_y (red) and v_z (green)

bin for each of the three directions and normalized it by the maximum velocity.

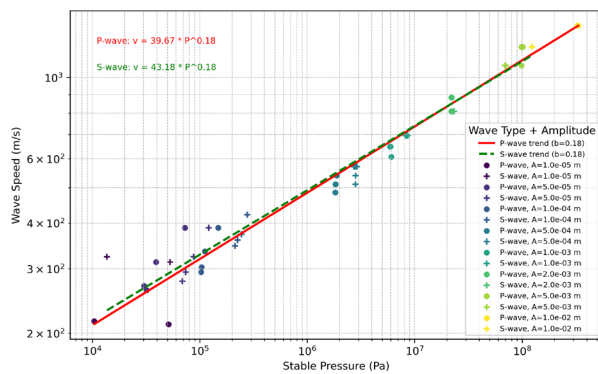


Figure 7. Log–log plot of P- and S-wave velocities versus stable pressure at different excitation amplitudes. Both wave types follow nearly identical straight-line trends, revealing a power-law relationship across the sampled pressure range. The nearly overlapping slopes indicate a transition of an S wave into a P wave.

We observed (Figure 6) that beyond the top bins (20–25), both the P and S wave velocity envelopes coincide for each pressure and pulse amplitude, with the v_y component dominating, which indicates that the S wave transitions into a P wave.

Figure 7 shows further evidence for the transition of a P wave into an S wave. The figure shows that the wave velocity only depends on stable pressure (the sum of confining and induced pressure), independent of the method

of pulse excitation, longitudinal for P waves and lateral for S waves.

5 Conclusion

We have performed simulations for constant velocity compression and short sinusoidal pulses. These simulations indicated a very weak dependence of the wave velocity on the confining pressure, as claimed in [1]. We also observed similar velocities for P and S pulses and, on further investigation, found that this might be due to the transition of an S pulse into a P pulse after the first few grain layers in the granular column. The role of the geometry of the column and the boundary conditions remains to be fully investigated.

References

- [1] Paul Sánchez et al *Planet. Sci. J.* **3** 245 (2022) <https://doi.org/10.3847/PSJ/ac960c>
- [2] A.P. Thompson et al., LAMMPS - a flexible simulation tool. *Comput. Phys. Commun.* **271**, 108171 (2022). <https://doi.org/10.1016/j.cpc.2021.108171>
- [3] D. Antypov and J. A. Elliott, “On an analytical solution for the damped Hertzian spring.” *Europhys. Lett.* **94**(5), 50004 (2011). <https://doi.org/10.1209/0295-5075/94/50004>
- [4] L. D. Landau and E. M. Lifshitz, *Theory of Elasticity*, Elsevier Ltd., Amsterdam, Netherlands (1986). <https://doi.org/10.1016/C2009-0-25521-8>